Data report: raw and normalized elemental data along the Site U1335, U1336, and U1337 splices from X-ray fluorescence scanning[1]

Julia K. Shackford,[2] Mitchell Lyle,[2] Roy Wilkens,[3] and Jun Tian[4]

Chapter contents

[1] Shackford, J.K., Lyle, M., Wilkens, R., and Tian, J., 2014. Data report: raw and normalized elemental data along the Site U1335, U1336, and U1337 splices from X-ray fluorescence scanning. *In* Pälike, H., Lyle, M., Nishi, H., Raffi, I., Gamage, K., Klaus, A., and the Expedition 320/321 Scientists, *Proc. IODP,* 320/321: Tokyo (Integrated Ocean Drilling Program Management International, Inc.). doi:10.2204/iodp.proc.320321.216.2014
[2] College of Geosciences, Texas A&M University, MS3146, Oceanography and Meteorology Building, College Station TX 77843, USA. Correspondence author: jkshackford@ocean.tamu.edu
[3] Hawaii Institute of Geophysics and Planetology, University of Hawaii at Manoa, 1680 East West Road, Honolulu HI 96822, USA.
[4] Laboratory of Marine Geology, Tongji University, Siping Road 1239, Shanghai 200092, P.R.China.

Abstract

We used X-ray fluorescence (XRF) scanning on samples from Integrated Ocean Drilling Program Expeditions 320/321 Sites U1335–U1337 to measure sediment geochemical compositions at 2.5 and 5 cm resolution for a total of 937 m of spliced sediment column. Site U1335 was scanned from 0 to 302 meters composite depth (mcd), Site U1336 was scanned from 0 to 142.5 mcd, and Site U1337 was scanned from 0 to 491.6 mcd, which is the entire splice. Here we report the data and describe the data acquisition conditions to measure Al, Si, K, Ca, Ti, Mn, Fe, and Ba in the solid phase. We also describe a method to convert data from volume-based raw XRF scan data to a normalized mass measurement, ready for calibration by other geochemical methods. Both the raw and normalized data are reported along each of the splices for Sites U1335–U1337.

Introduction

One primary objective of the Integrated Ocean Drilling Program (IODP) Pacific Equatorial Age Transect (PEAT) project is to produce continuous records tracking the effects of climate change in the eastern equatorial Pacific with enough detail to resolve orbitally forced climate cycles. A significant part of climate change is recorded by variability in the chemical composition of sediment, but this information is typically difficult to extract at a reasonable cost (see the **"Methods"** chapter [Expedition 320/321 Scientists, 2010a]).

X-ray fluorescence (XRF) scanning is an economical and nondestructive way to extract chemical data from split cores. XRF scanning is an X-ray optical technique that can measure the majority of the major elements and some minor elements in ~20–30 s per measurement. The vertical spacing at which data were collected for this project is similar to that at which physical properties were gathered on board the ship. The chemical measurements collected from XRF scanning can supplement physical properties measurements to study cyclostratigraphy. If calibrated, XRF scan data can be used to understand the long-term evolution of biogeochemical cycles.

In this data report, we present the results of XRF scanning on the spliced sedimentary sections from Sites U1335–U1337 and describe a basic technique, following **Lyle et al.** (2012), used to nor-

doi:10.2204/iodp.proc.320321.216.2014

malize the data for further geochemical study. Both the raw and normalized data along the splices are presented in Tables T1, T2, and T3. We report depth in meters composite depth (mcd) using core composite depth below seafloor (CCSF-A) methodology (see the "Methods" chapter [Expedition 320/321 Scientists, 2010a]). Data at this sampling resolution collected from multiple cores along the transect, along with previously published data from Site U1338 (Lyle et al., 2012; Lyle and Backman, 2013), allow the study of geochemical cycles for long periods of time and across great distances in the eastern equatorial Pacific. Such data can be used to study how biogeochemical changes in the equatorial Pacific are related to long-term changes in global climate.

Site locations

The three sites in this data report, along with Site U1338, contain the major Neogene sediment sections for the PEAT equatorial Pacific megasplice. The sites are located between 7°42′N and 3°50′N (Fig. F1).

Site U1335

Site U1335 (5°18.735′N, 126°17.002′W; 4327.5 m water depth) is on ~26 Ma crust halfway between Site U1336, ~340 km to the northwest, and Site U1337, ~390 km to the southeast, and ~250 km south of the Clipperton Fracture Zone (see the "Site U1335" chapter [Expedition 320/321 Scientists, 2010b]). This site is located on a broad plateau that parallels the Clipperton Fracture Zone and is within north-northeast–trending abyssal hill topography. Drilling recovered 417 m of biogenic sediment above basement. Here we report XRF scan data at 2.5 cm spacing for only part of the Site U1335 splice, from 0 to 302.66 mcd, covering the time span between ~0 and 20 Ma. Figure F2 shows $CaCO_3$ normalized median-squared (NMS) data from 0 to 302.66 mcd.

Site U1336

Site U1336 (7°42.067′N, 128°15.253′W; 4286 m water depth) is on 32 Ma crust, ~340 km northwest of Site U1335 (see the "Site U1336" chapter [Expedition 320/321 Scientists, 2010c]). The site is ~30 km north of the center of the Clipperton Fracture Zone on a local high that is draped with ~300 m of sediment cover. The abyssal hills are oriented slightly west of due north. Coring revealed a hiatus at the top of the section to ~12 Ma. Here we report XRF scan data at 2.5 cm spacing for only part of the Site U1336 splice, from 0 to 142.46 mcd. The Site U1336 scanning covers an age span roughly from 12 Ma (the top of the sediment column) to 22 Ma. The splice used for this project is a revised version of the shipboard splice based on Wilkens et al. (2013). The revisions are due primarily to a poorly recovered interval at roughly 152 mcd that resulted in cores being appended to one another below this depth, rather than being tied together. The appended interval is below the scanned interval. Figure F3 shows $CaCO_3$ NMS data from 0 to 142.46 mcd.

Site U1337

Site U1337 (3°50.009′N, 123°12.352′W; 4463 m water depth) is on ~24 Ma crust between the Galapagos and Clipperton Fracture Zones (see the "Site U1337" chapter [Expedition 320/321 Scientists, 2010d]). The site is ~390 km southeast of Site U1335, on a plateau between higher topography south of the site and a ridge to the north. Here we report XRF scan data for the entire Site U1337 splice, from 0 to 491.62 mcd, covering the entire spliced section. The upper sediment column (0–102.45 cm along the splice) was scanned at 5 cm intervals in order to tie to the high-resolution scan (0.5 cm interval) scanned by K. Iijima (unpubl. data). The remainder of the sediment column was scanned at 2.5 cm spacing. The splice we use has some changes from the original shipboard splice due to core disturbance, especially at greater depth, and trouble with correlating the four cores that make up the Site U1337 splice. The splice is the revised splice reported in Wilkens et al. (2013). A depth of close to 490 mcd was reached with only three gaps from the four holes. Figure F4 shows $CaCO_3$ NMS from 0 to 475 mcd for Site U1337.

XRF scanning of Site U1335–U1337 spliced sections

Sites U1335–U1337 exhibit the characteristic variations in sedimentary calcium carbonate content that result in the common seismic stratigraphy found throughout the equatorial Pacific east of Hawaii (Mayer et al., 1986). It has been difficult in the past to understand and determine what forcing mechanisms caused these carbonate cycles, which in turn caused these common seismic horizons, because they were poorly resolved by low-resolution shipboard sampling and analysis. Through the use of XRF scanning and discrete geochemical sampling to calibrate the XRF scan data, we can potentially determine calcium carbonate content, biogenic opal, biogenic barium (bio-Ba), and clay content in fine enough detail to better understand why sedimentary carbonate has varied in the equatorial Pacific.

XRF scanning can be used to study the biogeochemically active elements Ca, Si, and Ba in order to un-

derstand changes in productivity (Lyle et al., 2012). These data can then be compared to changes in preservation to further understand changes in the overall carbon cycle. XRF scan data can also be used to measure aluminosilicate elements including Al, K, and Ti to better understand the dust input to the region (Lyle et al., 2012). Measuring redox-sensitive elements such as Fe and Mn gives information about the sedimentary redox environment, as well as a measure of distal hydrothermal plume deposition near the basement (Lyle et al., 2012).

XRF uses the characteristic fluorescence of elements exposed to high-energy X-ray illumination to estimate a sample's chemical composition. High-energy X-ray photons eject inner-shell electrons from atoms being illuminated by the X-rays (Jansen et al., 1998), and the vacancies are filled by outer shell electrons. The excess energy is released as characteristic X-ray fluorescence energies for each element. The intensity of the fluorescence can be used to determine the abundance of different elements within the illuminated sample. With a scanning XRF, the detector is moved by a stepping system along a sediment core so that multiple measurements can be taken automatically (Richter et al., 2006).

Methods and materials

The spliced sediment columns from Sites U1335–U1337 were scanned using the third-generation Avaatech XRF scanner at the IODP Gulf Coast Repository in College Station, Texas (USA) (odases.tamu.edu/index.php/research-facilities/). This XRF scanner is equipped with a Canberra X-PIPS SDD, model SXD 15C-150-500 150 eV resolution X-ray detector and uses an X-ray tube with a Rh-anode to generate the incident X-rays that illuminate the sample. The XRF scanner is configured to analyze split sediment core halves for elements between Al and U on the periodic table. The X-ray tube and detector are mounted on a moving track so that multiple spots at different depths can be analyzed on a split core during the scanning run, and multiple scans with different settings can be programmed to run automatically (Richter et al., 2006). There are, however, parameters controlled by the operator, such as X-ray tube current, voltage, measurement time (live time), filters, and area of X-ray illumination. The downcore position step is precise to 0.1 mm.

XRF scanning

Sample spacing along each of the Site U1335 and U1336 core sections was set at 2.5 cm. For Site U1337, sample spacing was set at 2.5 cm in the lower spliced section and 5 cm in the 0–110 mcd section overlapping with K. Iijima's (unpubl. data) work. Two separate scans at different voltages were used on each section to gather all chemical data. The first scan was performed at 10 kV with no filter for Al, Si, S, Cl, K, Ca, Ti, Mn, and Fe. The measurement (live) time was set at 30 s, and the X-ray tube current was set to at 500 µA. A second scan for Ba was performed at 50 kV with a Cu filter, a measurement time of 10 s, and the X-ray tube current set to 1000 µA. We lowered the X-ray tube current from 2000 µA used for the Site U1338 scanning (Lyle et al., 2012) in order to preserve tube life and reduce the possibility of peak overlap problems. The core face illuminated by X-rays was set at 1.0 cm in the downcore direction and 1.2 cm in the cross-core direction.

For the Site U1335 and U1337 cores, the scans were run down the center of the split core half (6.8 cm total diameter). For the Site U1336 cores, the majority of the scans were run down the left side of the split core half to avoid the U-channel gap left by sampling for magnetostratigraphic analyses on the archive core prior to the XRF scanner runs. On the U-channeled sections, the track in the XRF core scanner was offset ~3 cm from the core's centerline. Additionally, cracks and holes from sampling in any of the cores were skipped if they corresponded to XRF sample spacing.

Each core was removed from refrigeration a minimum of 8 h prior to scanning to allow it to warm to room temperature. Each section was then covered ~15 min prior to scanning with 4 µm thick Ultralene plastic film (SPEX Centriprep, Inc.) to protect the detector face from becoming contaminated during the scan. Following the methods in Lyle et al. (2012), the Ultralene film was placed over the core sections only once they had warmed to room temperature in order to avoid condensation building up on the film while the core sections warmed. Condensation buildup can lead to severely reduced light element (e.g., Al and Si) XRF peak areas because of the condensation absorbing the low-energy X-ray fluorescence coming back from the sediment to the detector (Tjallingii et al., 2007).

There were a few unexplained data dropouts that we found after plotting the data, one and occasionally two data points that were significantly lower than the data trends of the scan. Where we had overlapping data, we found these "events" on only one of the overlapping sections. We attribute the dropouts to an intermittent instrument failure and removed them from the data sets, including those shown in Tables T1, T2, and T3. We found 15 bad data points between 109 and 114 mcd in the Site U1336 core sections. Of the 15 bad data points found in the Site

U1336 splice, 7 were outside of the splice, meaning they were in the overlapped section and would not have been included in the final splice even if they were kept, and 8 were within the splice, meaning that they would have been included in the final splice. All 15 bad data points were removed. Two additional bad data points were found in the Site U1336 splice at ~32 and ~83 mcd. Both of these points were removed as well.

Sediment splices

XRF scanning was done to cores along the sediment splices, not to all sections recovered from the different holes at each site. Only core sections along the continuous spliced sections of Sites U1335 and U1336 were analyzed. We scanned every archive core half included on the Site U1336 and U1337 splice tables in 2011 and 2012 and completed the scanning of the Site U1335 spliced sections in January 2013. If the splice transferred from one hole to the next in the middle of a section, both sections were run in their entirety to provide enough overlap to allow for the record to be adjusted, if needed. In the Site U1337 splice, substantial changes have been made to the original continuous splice table, so additional sections were run to aid in revising that record.

Tables **T1, T2,** and **T3** contain all of the data collected, not just the data that were used to construct the final splice (also see XRF in **"Supplementary material"**). Data incorporated into the splice are marked for easy extraction. Each table includes raw XRF peak area data and NMS reduced data for all three cores. Depths are indicated in meters below seafloor (mbsf), which is equivalent to core depth below seafloor (CSF-A), as well as converted to mcd, which is equivalent to CCSF-A. References to depth throughout this manuscript are in mcd. Medians of shipboard geochemical data and calculated area medians, both used in scaling and normalizing the raw XRF area data, are presented in Table **T4.** For each element in Tables **T1, T2,** and **T3,** we have listed the raw XRF peak area, the median-scaled total, and the NMS data as described below.

XRF data reduction

Data reduction was accomplished by a three-step method generally following the methods in **Lyle et al.** (2012). In the first step, which is an addition to the two-step reduction method developed in **Lyle et al.** (2012), negative peak area values were set to zero and removed from further calculations. Negative peak areas can appear where there are overlapping peaks and the elemental concentration is low. In this case, the measured data are actually below the modeled energy curve at 0 concentration.

Second, data were scaled by the median shipboard-measured bulk sediment elemental composition in order to scale elemental peak areas into typical ranges of sediment composition. Finally, the scaled components were summed and normalized to 100% in order to account for changes in porosity and cracks throughout the core sections. Only sections used in the final splices were used in calculating the area medians, so changes to the final splices may require recalculation of those medians and therefore NMS values.

To scale the XRF data, the following equation from **Lyle et al.** (2012), was used:

$$S_e = \text{Med}\%_e \times (\text{PeakArea}_e/\text{PeakArea}_{e,\text{med}}),$$

where S_e is the elemental scaling, $\text{Med}\%_e$ is the median weight percent of a sedimentary component, which was the oxide for each element (e.g., for Al, we used the oxide Al_2O_3, and for Ca, $CaCO_3$) from shipboard geochemical data, PeakArea_e is the measured elemental peak area in the sample, and $\text{PeakArea}_{e,\text{med}}$ is the median peak area over the data set.

To normalize the scaled XRF data, thereby removing the volume effect, each component (C) was multiplied by 100/(raw sum) to bring the total sum of components to 100%, rather than the lower value that results from high porosity or cracks:

$$\text{NMS}_c = C \times 100/(\text{raw sum}),$$

where NMS_c is the normalized median-scaled value for the component and C is the median-scaled value of the component. The sedimentary components in these data sets are Al_2O_3, SiO_2, K_2O, $CaCO_3$, TiO_2, MnO, Fe_2O_3, and $BaSO_4$. Normalization minimizes the high-frequency noise produced from greater porosity in the shallower portions of the splice and increased cracks and uneven surfaces in the lower sections of the splice.

Through the scaling and normalization process, we developed a way to quantitatively estimate sediment concentration based on XRF scans. XRF NMS estimates, however, can have significant errors if the model of sediment composition (the "type" of sediment composition) used is very different from the actual sediment composition. In other words, errors will result if the model sediment components do not match those within the actual sediment (e.g., if Ca is found in a clay and thus would be better represented by a CaO component) or if a major element found in the sediment is not included in the model. Despite these issues, NMS data are significantly better to study the changes in sediment composition than the raw XRF peak area because the porosity effect is re-

moved. Raw peak area data can have larger relative errors because of the differences in porosity between the sediment layers and from technical problems landing the detector on a flat sediment surface. Very dry and cracked sediment can cause the detector to not land flat against the sediment while collecting peak area data, or to have small cracks included in the scan area, lowering the raw counts. Figure F5 shows the raw median-scaled $CaCO_3$, the NMS $CaCO_3$, and discrete $CaCO_3$ for Sites U1335–U1337. Scaling and normalization reduced apparent noise in the XRF data and made the total range more similar to the variability seen in the shipboard data.

The NMS data can be easily calibrated to estimated sediment composition by analyzing a small set of check data that spans the typical range of sediment values and correlating the NMS data to the discrete measurements (Lyle and Backman, 2013).

Results

One of the important uses of XRF scanning is to be able to produce high-resolution data sets, such as the >19 m.y. sediment records from Sites U1335 and U1337. The Site U1336 sediment record spans ~12.12 to 20 Ma. Figure F6 shows the NMS time series of $CaCO_3$ NMS data at all three sites examined in this study. Also shown are biostratigraphic and magnetostratigraphic tie lines used to compare the records at each site to one another. Table T5 provides the depths, ages, and types of stratigraphic tie points shown in the figure. The upper section of the Site U1337 splice is expanded when compared with that of the Site U1335 splice because Site U1337 has been in closer proximity to the Equator since 12 Ma (1.1°–3.8°N) versus 2.4°–5.3°N for Site U1335. The closer proximity to the Equator exposed Site U1337 to higher sediment deposition. As the sites moved further from the Equator, they received less sediment deposition, as illustrated in the extreme by the hiatus from ~0 to 12 Ma at Site U1336.

Figure F7 shows all three sites, again with bio- and magnetostratigraphic tie lines, focusing on a very prominent $CaCO_3$ low that peaks at ~17 Ma and begins at ~17.7 Ma. The age is earlier than the usually assumed start of the Monterey carbon isotope excursion (16.9–13.7 Ma; Holbourn et al., 2007) but older than that of the Columbia River basalt flood basalt eruption (~16.8–5.5 Ma; Reidel and Tolan, 2013), which could have released significant amount of deep CO_2 that potentially could have caused added carbonate dissolution in the oceans. The peak $CaCO_3$ dissolution occurs at or slightly after the onset of the southeast Oregon eruptions that began the deposition of the Columbia River basalts in North America (16.8–16.6 Ma; Barry et al., 2013). The flood basalt deposition and the equatorial Pacific dissolution event can only be linked if volatile degassing is associated with the emplacement of the magma in the crust, not the eruption.

The 17 Ma carbonate dissolution event lasted ~1 m.y. and is strongly influenced by orbital insolation changes. The $CaCO_3$ analyses indicate cyclicity on an approximately 100,000 y timescale.

Conclusions

We present scanning XRF data along the splices of Sites U1335–U1337 (41,925 total sample measurements, with 33,739 samples along the three splices) and show their use in exploring the history of the equatorial Pacific productivity zone. We found we could scan the splices for Al, Si, K, Ca, Ti, Mn, Fe, and Ba in a reasonably short amount of time, averaging slightly more than 1 h per section. The raw data, however, are a volume measurement and must be scaled, normalized, and eventually calibrated to make an estimate of sediment composition. The NMS data-reduction process described helps to make correlations between raw peak areas and measured chemical compositions more linear so that calibration is easier. To achieve good results, care must be taken to choose a sediment compositional model (median composition and type of sediment components) that is similar to the sediment under investigation. Calibration is the final step in converting XRF scan data to a compositional estimate. Ideally, enough samples are measured by discrete geochemical analysis that some of the data are left out of the calibration and can be used to check the data.

Acknowledgments

We thank Integrated Ocean Drilling Program (IODP) Expedition 320/321 party members, IODP, and the IODP Gulf Coast Repository (GCR) for providing samples and assistance during XRF analysis, as well as all the effort they put in to properly collect and archive the Site U1335–U1337 sediment cores. Additionally, we would like to thank the reviewers for their constructive comments and assistance. We also acknowledge the Ocean Drilling and Sustainable Earth Sciences (ODASES) program at Texas A&M University for acquiring the Avaatech XRF scanner for the GCR, as well as for fellowship funding for J. Shackford. Scanning and analysis were paid for by a United States Advisory Committee for Scientific Ocean Drilling postcruise grant and by National Science Foundation grant OCE-0962184 to M. Lyle.

References

Barry, T.L., Self, S., Kelley, S.P., Reidel, S., Hooper, P., and Widdowson, M., 2010. New $^{40}Ar/^{39}Ar$ dating of the Grande Ronde lavas, Columbia River basalts, USA: implications for duration of flood basalt eruption episodes. *Lithos,* 118(3–4):213–222. **doi:10.1016/j.lithos.2010.03.014**

Expedition 320/321 Scientists, 2010a. Methods. *In* Pälike, H., Lyle, M., Nishi, H., Raffi, I., Gamage, K., Klaus, A., and the Expedition 320/321 Scientists, *Proc. IODP,* 320/321: Tokyo (Integrated Ocean Drilling Program Management International, Inc.). **doi:10.2204/iodp.proc.320321.102.2010**

Expedition 320/321 Scientists, 2010b. Site U1335. *In* Pälike, H., Lyle, M., Nishi, H., Raffi, I., Gamage, K., Klaus, A., and the Expedition 320/321 Scientists, *Proc. IODP,* 320/321: Tokyo (Integrated Ocean Drilling Program Management International, Inc.). **doi:10.2204/iodp.proc.320321.107.2010**

Expedition 320/321 Scientists, 2010c. Site U1336. *In* Pälike, H., Lyle, M., Nishi, H., Raffi, I., Gamage, K., Klaus, A., and the Expedition 320/321 Scientists, *Proc. IODP,* 320/321: Tokyo (Integrated Ocean Drilling Program Management International, Inc.). **doi:10.2204/iodp.proc.320321.108.2010**

Expedition 320/321 Scientists, 2010d. Site U1337. *In* Pälike, H., Lyle, M., Nishi, H., Raffi, I., Gamage, K., Klaus, A., and the Expedition 320/321 Scientists, *Proc. IODP,* 320/321: Tokyo (Integrated Ocean Drilling Program Management International, Inc.). **doi:10.2204/iodp.proc.320321.109.2010**

Holbourn, A., Kuhnt, W., Schulz, M., Flores, J.-A., and Andersen, N., 2007. Orbitally-paced climate evolution during the middle Miocene "Monterey" carbon-isotope excursion. *Earth Planet. Sci. Lett.,* 261(3–4):534–550. **doi:10.1016/j.epsl.2007.07.026**

Jansen, J.H.F., Van der Gaast, S.J., Koster, B., and Vaars, A.J., 1998. CORTEX, a shipboard XRF-scanner for element analyses in split sediment cores. *Mar. Geol.,* 151(1–4):143–153. **doi:10.1016/S0025-3227(98)00074-7**

Lyle, M., and Backman, J., 2013. Data report: calibration of XRF-estimated $CaCO_3$ along the Site U1338 splice. *In* Pälike, H., Lyle, M., Nishi, H., Raffi, I., Gamage, K., Klaus, A., and the Expedition 320/321 Scientists, *Proc. IODP,* 320/321: Tokyo (Integrated Ocean Drilling Program Management International, Inc.). **doi:10.2204/iodp.proc.320321.205.2013**

Lyle, M., Olivarez Lyle, A., Gorgas, T., Holbourn, A., Westerhold, T., Hathorne, E., Kimoto, K., and Yamamoto, S., 2012. Data report: raw and normalized elemental data along the Site U1338 splice from X-ray fluorescence scanning. *In* Pälike, H., Lyle, M., Nishi, H., Raffi, I., Gamage, K., Klaus, A., and the Expedition 320/321 Scientists, *Proc. IODP,* 320/321: Tokyo (Integrated Ocean Drilling Program Management International, Inc.). **doi:10.2204/iodp.proc.320321.203.2012**

Mayer, L.A., Shipley, T.H., and Winterer, E.L., 1986. Equatorial Pacific seismic reflectors as indicators of global oceanographic events. *Science,* 233(4765):761–764. **doi:10.1126/science.233.4765.761**

Pälike, H., Nishi, H., Lyle, M., Raffi, I., Gamage, K., Klaus, A., and the Expedition 320/321 Scientists, 2010. Expedition 320/321 summary. *In* Pälike, H., Lyle, M., Nishi, H., Raffi, I., Gamage, K., Klaus, A., and the Expedition 320/321 Scientists, *Proc. IODP,* 320/321: Tokyo (Integrated Ocean Drilling Program Management International, Inc.). **doi:10.2204/iodp.proc.320321.101.2010**

Reidel, S.P., and Tolan, T.L., 2013. The late Cenozoic evolution of the Columbia River system in the Columbia River flood basalt province. *In* Reidel, S.P., Camp, V.E., Ross, M.E., Wolff, J.A., Martin, B.S., Tolan, T.L., and Wells, R.E. (Eds.), *The Columbia River Flood Basalt Province.* Spec. Pap.—Geol. Soc. Am., 497:201–230.

Richter, T.O., van der Gaast, S., Koster, B., Vaars, A., Gieles, R., de Stigter, H.C., De Haas, H., and van Weering, T.C.E., 2006. The Avaatech XRF Core Scanner: technical description and applications to NE Atlantic sediments. *In* Rothwell, R.G. (Ed.), *New Techniques in Sediment Core Analysis*. Geol. Soc. Spec. Publ., 267(1):39–50. **doi:10.1144/GSL.SP.2006.267.01.03**

Tjallingii, R., Röhl, U., Kölling, M., and Bickert, T., 2007. Influence of the water content on X-ray fluorescence core-scanning measurements in soft marine sediments. *Geochem., Geophys., Geosyst.,* 8(2):Q02004. **doi:10.1029/2006GC001393**

Wilkens, R.H., Dickens, G.R., Tian, J., Backman, J., and the Expedition 320/321 Scientists, 2013. Data report: revised composite depth scales for Sites U1336, U1337, and U1338. *In* Pälike, H., Lyle, M., Nishi, H., Raffi, I., Gamage, K., Klaus, A., and the Expedition 320/321 Scientists, *Proc. IODP,* 320/321: Tokyo (Integrated Ocean Drilling Program Management International, Inc.). **doi:10.2204/iodp.proc.320321.209.2013**

Initial receipt: 20 August 2013
Acceptance: 7 May 2014
Publication: 15 August 2014

Figure F1. Expedition 320/321 sites and Pacific Equatorial Age Transect drilling locations. Black circles are other sites drilled during Integrated Ocean Drilling Program, Deep Sea Drilling Project, and Ocean Drilling Program. F.Z. = fracture zone. From the **"Expedition 320/321 summary"** chapter (Pälike et al., 2010).

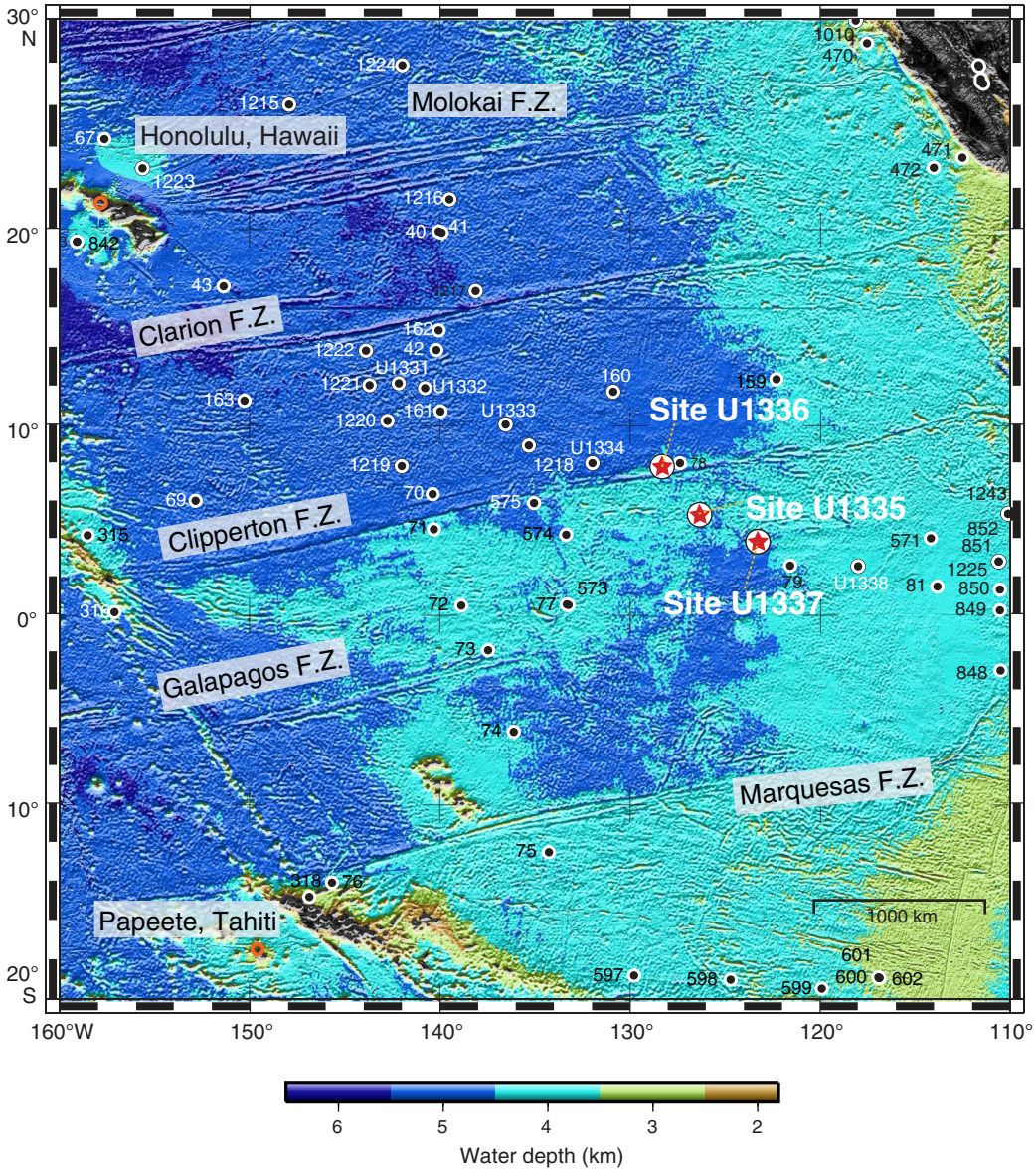

Figure F2. $CaCO_3$ normalized median-squared (NMS) values vs. depth, Site U1335.

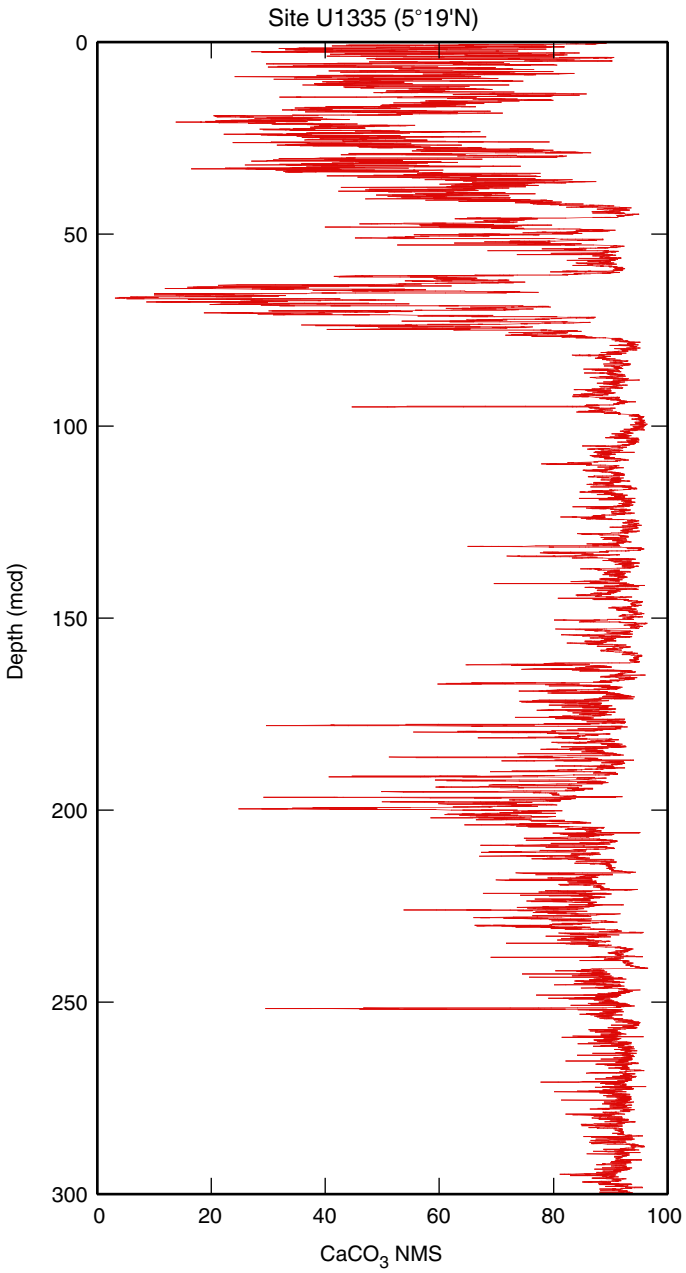

Figure F3. $CaCO_3$ normalized median-squared (NMS) values vs. depth, Site U1336.

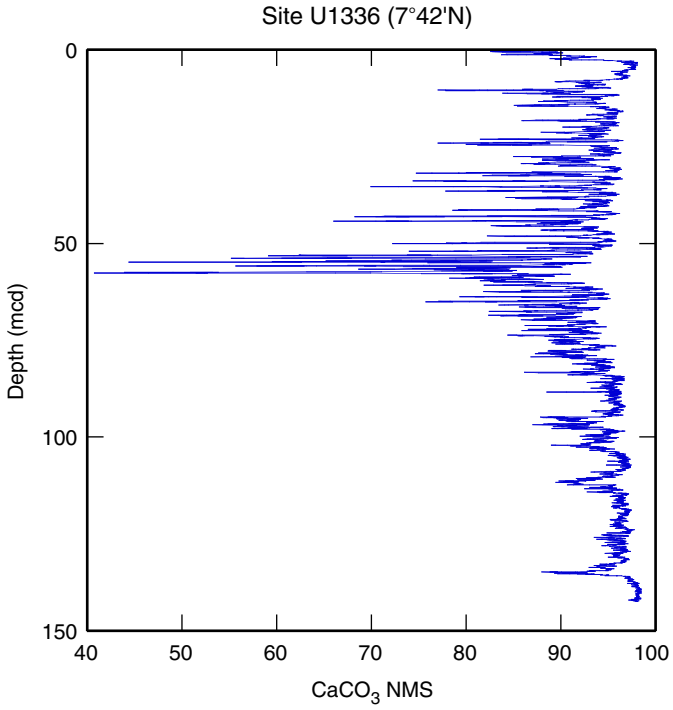

Figure F4. $CaCO_3$ normalized median-squared (NMS) values vs. depth, Site U1337.

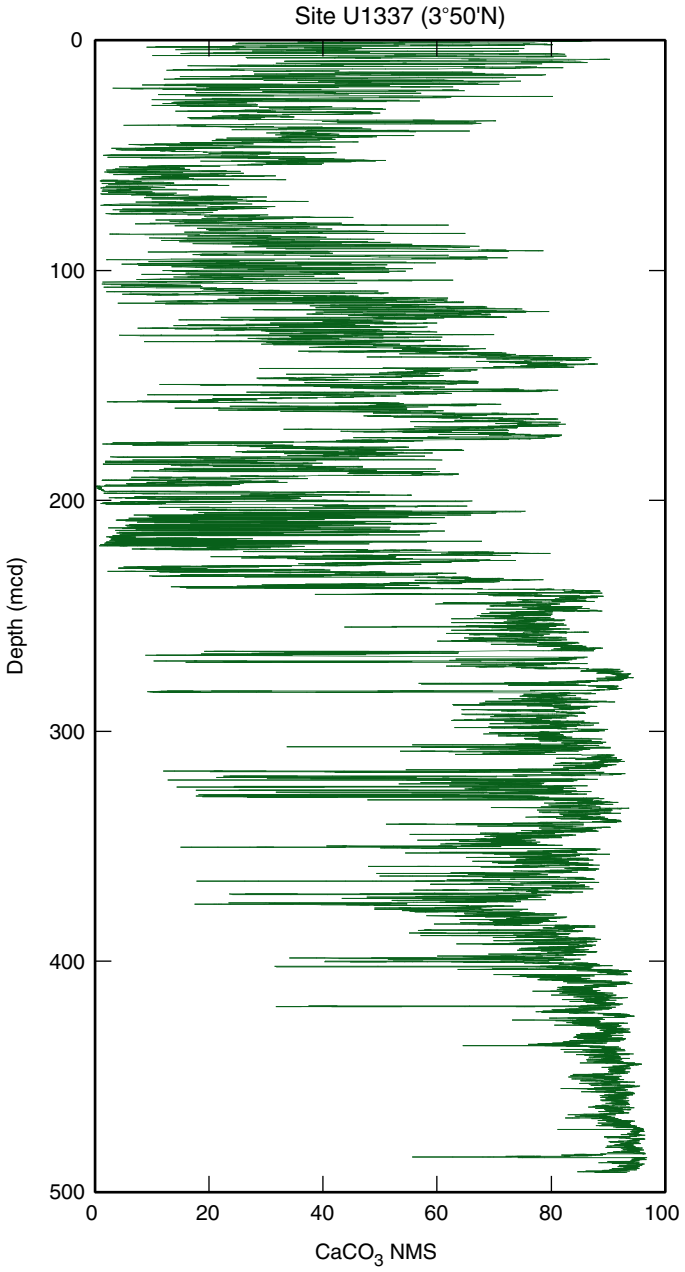

Figure F5. Comparison of raw median-scaled $CaCO_3$ with normalized median-squared (NMS) $CaCO_3$ estimates, discrete shipboard $CaCO_3$, and discrete shore-based $CaCO_3$ (Site U1337 only; J. Shackford, unpubl. data). Normalizing the sum of components to 100% removes the variability as well as corrects for volume effects.

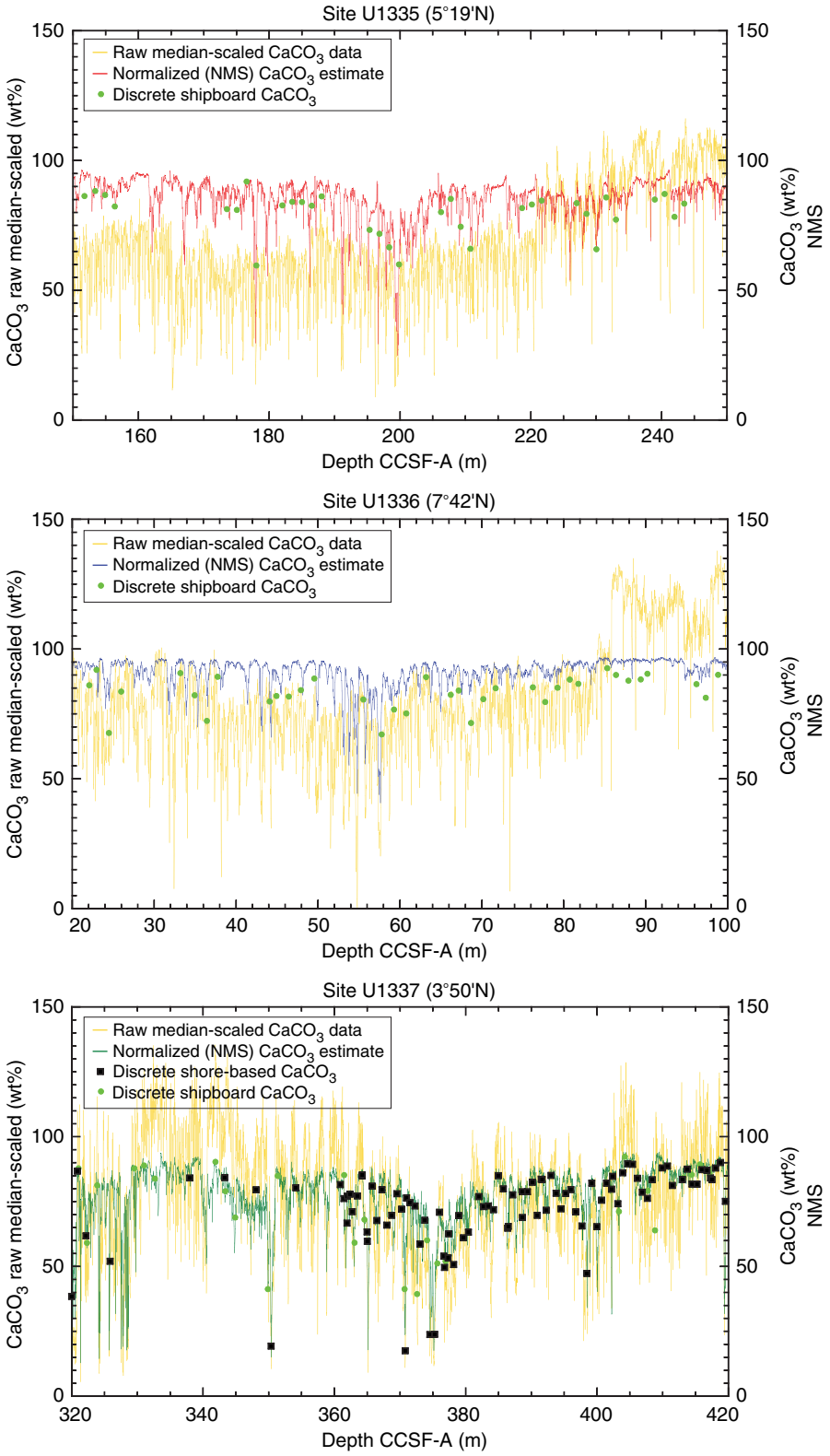

Figure F6. $CaCO_3$ normalized median-squared (NMS) values and stratigraphic correlation between Sites U1335, U1336, and U1337. Ages are shown above the stratigraphic tie lines.

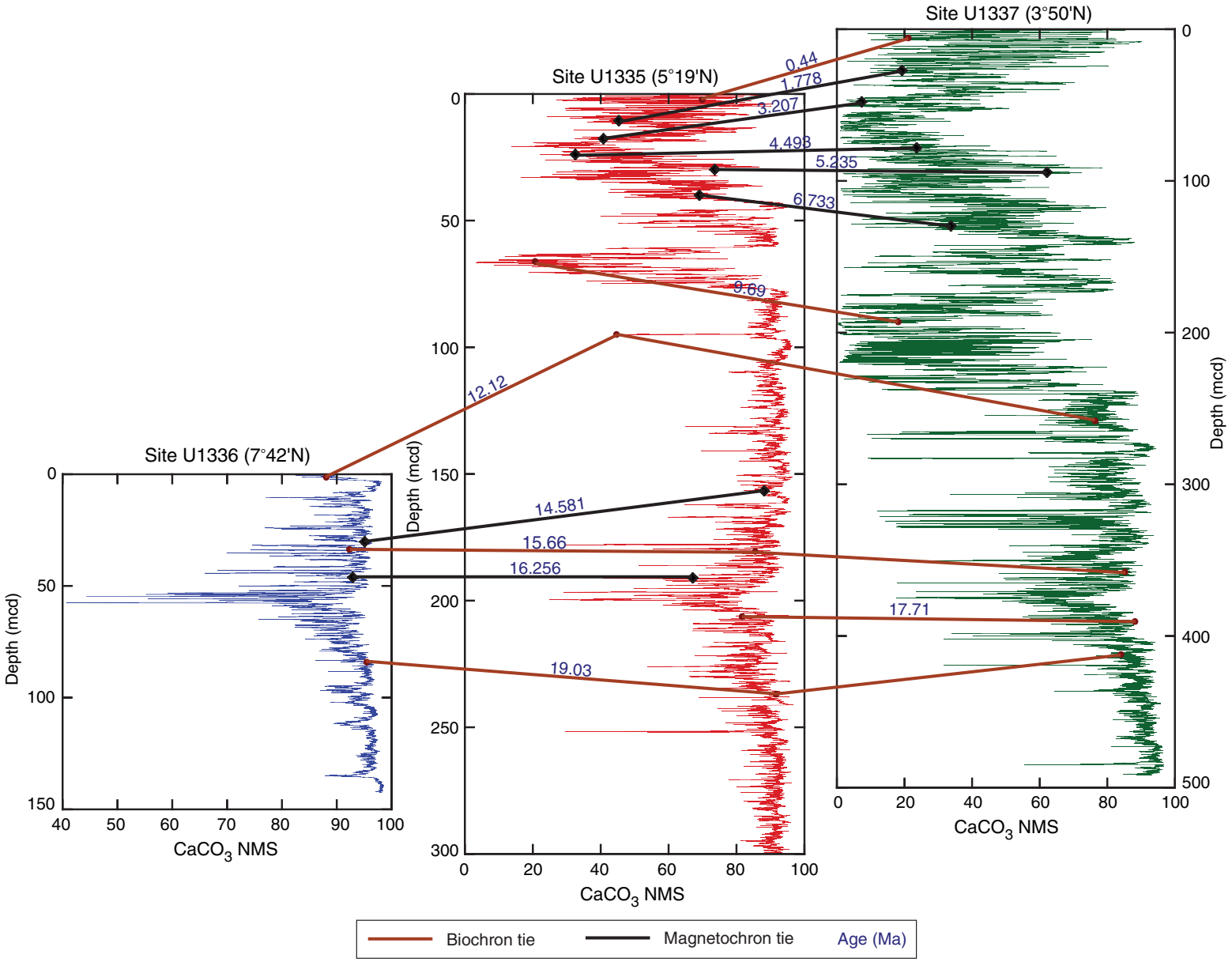

Figure F7. $CaCO_3$ normalized median-squared (NMS) values and stratigraphic correlation between Sites U1335, U1336, and U1337 for the period of time surrounding the 17 Ma $CaCO_3$ dissolution event. Ages are shown above the stratigraphic tie lines. Additionally, the primary $CaCO_3$ dissolution signal of the 17 Ma event is outlined by a yellow box.

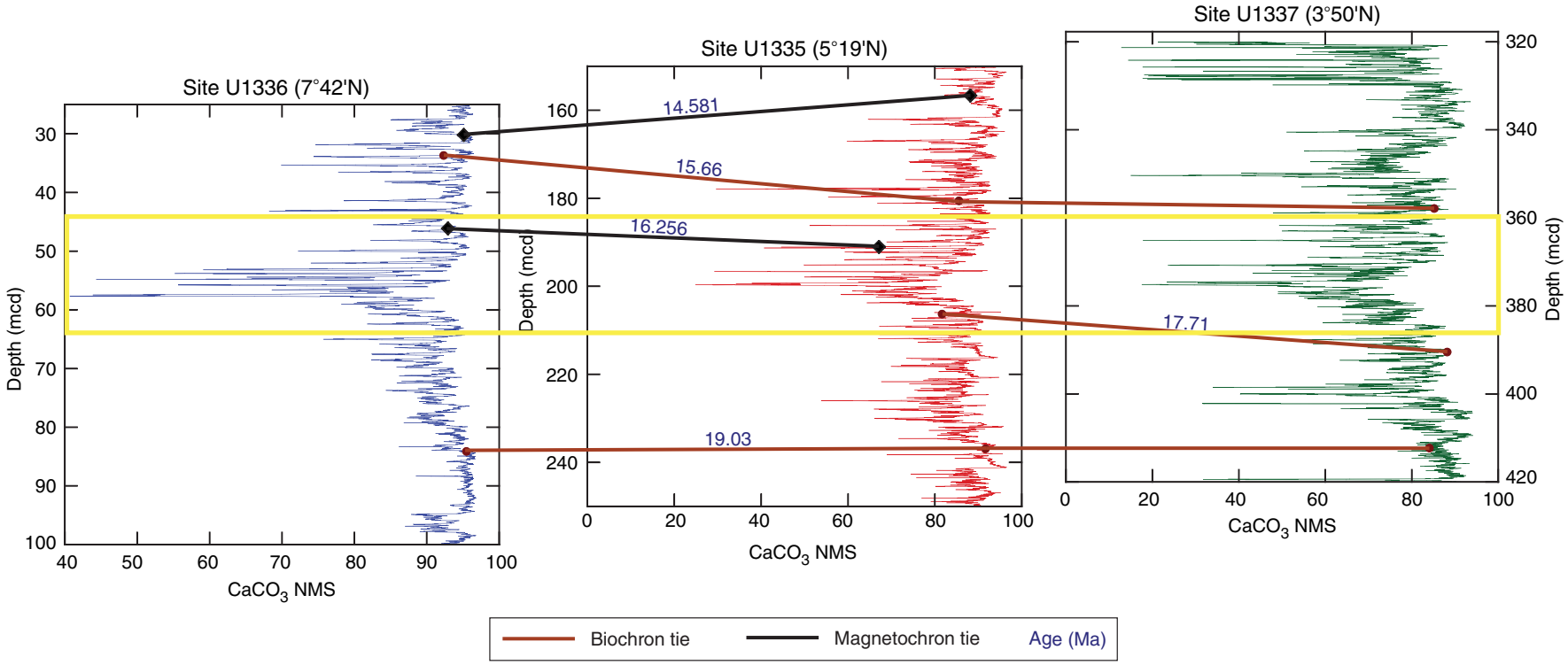

Table T1. Raw X-ray fluorescence peak area data and calculated normalized median-squared (NMS) spliced data for all scans, Site U1335.

Core, section	Depth in section (mm)	Measurement date	Depth (mbsf [m revised CSF-A])	Depth (mcd [m revised CCSF-A])	Raw component sum (%)	Al area	Al median-scale	Al_2O_3 NMS	Si area	Si median-scale	SiO_2 NMS	S area
320-U1335B-												
1H-1*	25	1/12/2013	0.025	0.025	36.67	64	0.12	0.32	21,039	5.79	15.78	3,461
1H-1*	50	1/12/2013	0.05	0.05	31.36	69	0.12	0.40	16,866	4.64	14.79	3,066
1H-1*	75	1/12/2013	0.075	0.075	36.51	16	0.03	0.08	15,265	4.20	11.50	3,076
1H-1*	100	1/12/2013	0.1	0.1	45.57	0	0.00	0.00	18,783	5.17	11.34	2,734
1H-1*	125	1/12/2013	0.125	0.125	47.06	0	0.00	0.00	20,625	5.67	12.05	3,361
1H-1*	150	1/12/2013	0.15	0.15	45.69	55	0.10	0.22	18,874	5.19	11.36	3,609
1H-1*	175	1/12/2013	0.175	0.175	65.34	14	0.03	0.04	29,423	8.09	12.39	5,432
1H-1*	200	1/12/2013	0.2	0.2	71.57	413	0.75	1.04	33,660	9.26	12.94	5,581
1H-1*	225	1/12/2013	0.225	0.225	70.91	107	0.19	0.27	30,863	8.49	11.97	6,382
1H-1*	250	1/12/2013	0.25	0.25	75.52	49	0.09	0.12	24,797	6.82	9.03	5,186
1H-1*	275	1/12/2013	0.275	0.275	72.30	286	0.52	0.72	25,641	7.05	9.75	5,439
1H-1*	300	1/12/2013	0.3	0.3	70.58	0	0.00	0.00	21,389	5.88	8.34	5,365
1H-1*	325	1/12/2013	0.325	0.325	65.62	0	0.00	0.00	20,307	5.59	8.51	5,204
1H-1*	350	1/12/2013	0.35	0.35	78.66	260	0.47	0.60	25,007	6.88	8.74	5,417
1H-1*	375	1/12/2013	0.375	0.375	74.17	185	0.33	0.45	23,231	6.39	8.61	6,270
1H-1*	400	1/12/2013	0.4	0.4	72.52	180	0.33	0.45	24,736	6.80	9.38	5,590
1H-1*	425	1/12/2013	0.425	0.425	65.83	114	0.21	0.31	23,627	6.50	9.87	5,521
1H-1*	450	1/12/2013	0.45	0.45	70.27	118	0.21	0.30	24,837	6.83	9.72	5,400
1H-1*	475	1/12/2013	0.475	0.475	68.32	286	0.52	0.76	26,155	7.19	10.53	5,740
1H-1*	500	1/12/2013	0.5	0.5	50.10	0	0.00	0.00	17,595	4.84	9.66	5,113
1H-1*	525	1/12/2013	0.525	0.525	51.57	150	0.27	0.53	20,473	5.63	10.92	5,525
1H-1*	550	1/12/2013	0.55	0.55	49.29	192	0.35	0.71	22,399	6.16	12.50	5,070
1H-1*	575	1/12/2013	0.575	0.575	43.06	217	0.39	0.91	21,885	6.02	13.98	4,324
1H-1*	600	1/12/2013	0.6	0.6	49.98	634	1.15	2.30	32,509	8.94	17.89	6,279
1H-1*	625	1/12/2013	0.625	0.625	44.56	303	0.55	1.23	23,529	6.47	14.52	6,344
1H-1*	650	1/12/2013	0.65	0.65	36.88	706	1.28	3.47	29,336	8.07	21.88	7,720
1H-1*	675	1/12/2013	0.675	0.675	46.17	763	1.38	2.99	34,085	9.37	20.31	7,016
1H-1*	700	1/12/2013	0.7	0.7	36.02	765	1.38	3.84	35,422	9.74	27.05	8,347
1H-1*	725	1/12/2013	0.725	0.725	45.37	831	1.50	3.32	37,437	10.30	22.70	7,382
1H-1*	750	1/12/2013	0.75	0.75	44.58	1,500	2.72	6.09	53,036	14.59	32.72	8,838
1H-1*	775	1/12/2013	0.775	0.775	45.90	1,905	3.45	7.51	58,178	16.00	34.86	8,893
1H-1*	800	1/12/2013	0.8	0.8	52.74	1,740	3.15	5.97	53,884	14.82	28.10	8,585
1H-1*	825	1/12/2013	0.825	0.825	44.05	1,680	3.04	6.90	49,506	13.62	30.91	8,920
1H-1*	850	1/12/2013	0.85	0.85	39.81	1,704	3.08	7.75	49,828	13.70	34.42	8,610
1H-1*	875	1/12/2013	0.875	0.875	24.91	565	1.02	4.11	26,473	7.28	29.23	4,699
1H-1*	900	1/12/2013	0.9	0.9	23.76	448	0.81	3.41	23,878	6.57	27.64	4,458
1H-1*	925	1/12/2013	0.925	0.925	36.49	1,022	1.85	5.07	32,938	9.06	24.83	6,574
1H-1*	950	1/12/2013	0.95	0.95	22.02	746	1.35	6.13	26,576	7.31	33.19	4,439
1H-1*	975	1/12/2013	0.975	0.975	44.86	1,362	2.47	5.50	47,109	12.96	28.88	8,053
1H-1*	1,000	1/12/2013	1	1	53.54	1,398	2.53	4.73	44,589	12.26	22.91	7,993
1H-1*	1,025	1/12/2013	1.025	1.025	65.16	656	1.19	1.82	40,361	11.10	17.04	6,054
1H-1*	1,050	1/12/2013	1.05	1.05	65.54	522	0.95	1.44	36,649	10.08	15.38	6,243
1H-1*	1,075	1/12/2013	1.075	1.075	39.44	433	0.78	1.99	34,730	9.55	24.22	8,720
1H-1*	1,100	1/12/2013	1.1	1.1	64.91	527	0.95	1.47	36,322	9.99	15.39	6,415
1H-1*	1,125	1/12/2013	1.125	1.125	71.12	472	0.85	1.20	33,070	9.10	12.79	5,998
1H-1*	1,150	1/12/2013	1.15	1.15	76.64	581	1.05	1.37	37,704	10.37	13.53	5,236
1H-1*	1,175	1/12/2013	1.175	1.175	69.60	396	0.72	1.03	33,384	9.18	13.19	5,649
1H-1*	1,200	1/12/2013	1.2	1.2	65.85	381	0.69	1.05	31,416	8.64	13.12	5,053
1H-1*	1,225	1/12/2013	1.225	1.225	68.61	495	0.90	1.31	37,320	10.26	14.96	6,187
1H-1*	1,250	1/12/2013	1.25	1.25	58.88	635	1.15	1.95	39,681	10.91	18.54	6,613
1H-1*	1,275	1/12/2013	1.275	1.275	51.69	506	0.92	1.77	34,246	9.42	18.22	6,528
1H-1*	1,300	1/12/2013	1.3	1.3	27.08	182	0.33	1.22	15,827	4.35	16.07	2,722
1H-1*	1,325	1/12/2013	1.325	1.325	30.94	27	0.05	0.16	16,228	4.46	14.43	3,454
1H-1*	1,350	1/12/2013	1.35	1.35	43.13	2,485	4.50	10.43	21,238	5.84	13.54	8,300
1H-1*	1,375	1/12/2013	1.375	1.375	31.15	439	0.79	2.55	23,170	6.37	20.46	4,111
1H-1*	1,400	1/12/2013	1.4	1.4	49.07	1,009	1.83	3.72	41,887	11.52	23.48	6,968
1H-1*	1,425	1/12/2013	1.425	1.425	50.91	1,432	2.59	5.09	48,055	13.22	25.96	7,779
1H-1*	1,450	1/12/2013	1.45	1.45	50.27	2,033	3.68	7.32	57,543	15.83	31.48	9,262
1H-1*	1,475	1/12/2013	1.475	1.475	16.98	352	0.64	3.75	19,565	5.38	31.70	3,843
1H-2*	25	1/12/2013	1.525	1.525	34.16	420	0.76	2.23	26,857	7.39	21.62	4,261

* = data used in the calculation of NMS values and in the splice. All data are included, however, in the event that the splice is modified and NMS values need to be recalculated. Only a portion of this table appears here. The complete table is available in **ASCII** and in Microsoft Excel format (see RAWXRF_U1335.XLS in RAWXRF in **"Supplementary material."**)

Table T2. Raw X-ray fluorescence area data and calculated normalized median-squared (NMS) spliced data for all scans, Site U1336.

Core, section	Depth in section (mm)	Measurement date	Depth (mbsf [m revised CSF-A])	Depth (mcd [m revised CCSF-A])	Raw component sum (%)	Al area	Al median-scale	Al_2O_3 NMS	Si area	Si median-scale	SiO_2 NMS	S area
320-U1336B-												
1H-1*	25	1/26/2012	0.025	0.025	8.45	234	0.42	4.92	7,983	1.85	21.91	1,147
1H-1*	50	1/26/2012	0.05	0.05	21.98	515	0.91	4.16	17,624	4.09	18.59	1,727
1H-1*	75	1/26/2012	0.075	0.075	15.42	234	0.42	2.70	11,130	2.58	16.74	1,465
1H-1*	100	1/26/2012	0.1	0.1	16.38	326	0.58	3.54	12,401	2.87	17.56	1,625
1H-1*	125	1/26/2012	0.125	0.125	17.61	466	0.83	4.70	13,580	3.15	17.88	1,883
1H-1*	150	1/26/2012	0.15	0.15	18.61	624	1.11	5.96	16,311	3.78	20.32	2,408
1H-1*	175	1/26/2012	0.175	0.175	37.65	418	0.74	1.97	18,327	4.25	11.28	3,911
1H-1*	200	1/26/2012	0.2	0.2	40.61	291	0.52	1.27	20,255	4.70	11.56	4,031
1H-1*	225	1/26/2012	0.225	0.225	48.01	391	0.69	1.45	24,485	5.68	11.82	3,980
1H-1*	250	1/26/2012	0.25	0.25	53.40	419	0.74	1.39	23,143	5.37	10.05	4,435
1H-1*	275	1/26/2012	0.275	0.275	56.10	354	0.63	1.12	25,459	5.90	10.52	4,420
1H-1*	300	1/26/2012	0.3	0.3	62.71	257	0.46	0.73	22,320	5.17	8.25	3,174
1H-1*	325	1/26/2012	0.325	0.325	70.00	269	0.48	0.68	23,739	5.50	7.86	3,742
1H-1*	350	1/26/2012	0.35	0.35	70.40	307	0.55	0.77	22,399	5.19	7.38	4,117
1H-1*	375	1/26/2012	0.375	0.375	53.81	237	0.42	0.78	21,863	5.07	9.42	3,684
1H-1*	425	1/26/2012	0.425	0.425	51.82	307	0.55	1.05	22,083	5.12	9.88	3,220
1H-1*	450	1/26/2012	0.45	0.45	56.23	423	0.75	1.34	27,602	6.40	11.38	4,298
1H-1*	475	1/26/2012	0.475	0.475	58.35	602	1.07	1.83	30,017	6.96	11.93	4,250
1H-1*	500	1/26/2012	0.5	0.5	55.43	722	1.28	2.31	28,419	6.59	11.89	3,883
1H-1*	525	1/26/2012	0.525	0.525	55.74	425	0.75	1.35	24,976	5.79	10.39	4,104
1H-1*	550	1/26/2012	0.55	0.55	59.88	630	1.12	1.87	26,767	6.21	10.36	4,048
1H-1	575	1/26/2012	0.575	0.575	66.43	484	0.86	1.29	28,077	6.51	9.80	3,236
1H-1	600	1/26/2012	0.6	0.6	71.70	524	0.93	1.30	26,864	6.23	8.69	2,843
1H-1	625	1/26/2012	0.625	0.625	79.08	574	1.02	1.29	26,452	6.13	7.75	3,042
1H-1	650	1/26/2012	0.65	0.65	78.47	417	0.74	0.94	26,176	6.07	7.73	2,396
1H-1	675	1/26/2012	0.675	0.675	83.66	517	0.92	1.10	31,131	7.22	8.63	2,580
1H-1	700	1/26/2012	0.7	0.7	79.89	207	0.37	0.46	27,936	6.48	8.11	2,591
1H-1	725	1/26/2012	0.725	0.725	83.14	604	1.07	1.29	29,651	6.87	8.27	3,144
1H-1	750	1/26/2012	0.75	0.75	76.09	357	0.63	0.83	27,497	6.37	8.38	2,443
1H-1	775	1/26/2012	0.775	0.775	75.66	401	0.71	0.94	27,357	6.34	8.38	3,028
1H-1	800	1/26/2012	0.8	0.8	82.64	497	0.88	1.07	29,564	6.85	8.29	2,443
1H-1	825	1/26/2012	0.825	0.825	79.41	593	1.05	1.33	29,282	6.79	8.55	1,864
1H-1	850	1/26/2012	0.85	0.85	79.31	139	0.25	0.31	29,000	6.72	8.48	2,374
1H-1	875	1/26/2012	0.875	0.875	74.25	519	0.92	1.24	26,703	6.19	8.34	2,425
1H-1	900	1/26/2012	0.9	0.9	78.46	194	0.34	0.44	28,127	6.52	8.31	2,221
1H-1	925	1/26/2012	0.925	0.925	77.92	371	0.66	0.85	29,093	6.74	8.66	2,737
1H-1	950	1/26/2012	0.95	0.95	79.51	459	0.82	1.03	28,987	6.72	8.45	2,554
1H-1	975	1/26/2012	0.975	0.975	73.47	617	1.10	1.49	27,214	6.31	8.59	2,630
1H-1	1,000	1/26/2012	1	1	68.47	416	0.74	1.08	26,121	6.06	8.84	1,857
1H-1	1,025	1/26/2012	1.025	1.025	65.80	416	0.74	1.12	24,245	5.62	8.54	1,924
1H-1	1,050	1/26/2012	1.05	1.05	65.73	614	1.09	1.66	27,143	6.29	9.57	2,327
1H-1	1,075	1/26/2012	1.075	1.075	66.25	352	0.63	0.94	26,188	6.07	9.16	2,118
1H-1	1,100	1/26/2012	1.1	1.1	57.94	515	0.91	1.58	23,234	5.39	9.30	1,719
1H-1	1,125	1/26/2012	1.125	1.125	59.47	487	0.86	1.45	21,585	5.00	8.41	1,682
1H-1	1,150	1/26/2012	1.15	1.15	63.63	600	1.07	1.67	26,999	6.26	9.84	2,831
1H-1	1,175	1/26/2012	1.175	1.175	59.26	546	0.97	1.64	26,543	6.15	10.38	1,893
1H-1	1,200	1/26/2012	1.2	1.2	57.27	709	1.26	2.20	29,222	6.77	11.83	1,896
1H-1	1,225	1/26/2012	1.225	1.225	46.44	522	0.93	2.00	24,978	5.79	12.47	1,721
1H-1	1,275	1/26/2012	1.275	1.275	54.01	819	1.45	2.69	28,804	6.68	12.36	1,988
1H-1	1,300	1/26/2012	1.3	1.3	63.90	396	0.70	1.10	30,668	7.11	11.13	2,211
1H-1	1,325	1/26/2012	1.325	1.325	69.75	852	1.51	2.17	31,757	7.36	10.55	3,130
1H-1	1,350	1/26/2012	1.35	1.35	61.91	665	1.18	1.91	28,453	6.60	10.65	2,541
1H-1	1,375	1/26/2012	1.375	1.375	69.44	524	0.93	1.34	25,995	6.03	8.68	2,579
320/321-U1336A-												
1H-1	25	1/24/2012	0.025	0.285	19.16	413	0.73	3.83	16,539	3.83	20.01	1,842
1H-1	50	1/24/2012	0.05	0.31	38.92	979	1.74	4.47	27,221	6.31	16.22	2,812
1H-1	75	1/24/2012	0.075	0.335	26.51	732	1.30	4.90	21,279	4.93	18.61	2,396
1H-1	100	1/24/2012	0.1	0.36	27.86	1072	1.90	6.83	24,538	5.69	20.42	2,349
1H-1	125	1/24/2012	0.125	0.385	27.46	662	1.18	4.28	22,855	5.30	19.29	2,911

* = data used in the calculation of NMS values and in the splice. All data are included, however, in the event that the splice is modified and NMS values need to be recalculated. Only a portion of this table appears here. The complete table is available in **ASCII** and in Microsoft Excel format (see RAWXRF_U1336.XLS in RAWXRF in **"Supplementary material."**)

Table T3. Raw X-ray fluorescence area data and calculated normalized median-squared (NMS) spliced data for all scans, Site U1337.

Core, section	Depth in section (mm)	Measurement date	Depth (mbsf [m revised CSF-A])	Depth (mcd [m revised CCSF-A])	Raw component sum (%)	Al area	Al median-scale	Al_2O_3 NMS	Si area	Si median-scale	SiO_2 NMS	S area
321-U1337B-												
1H-1*	25	9/20/2012	1.025	0.025	51.55	280	0.71	1.37	28,368	15.11	29.32	6,694
1H-1*	50	9/20/2012	1.05	0.05	55.11	–59	0.00	0.00	25,856	13.77	24.99	9,528
1H-1*	75	9/20/2012	1.075	0.075	81.76	229	0.58	0.71	38,038	20.26	24.78	8,085
1H-1*	100	9/20/2012	1.1	0.1	70.87	404	1.02	1.44	41,109	21.90	30.90	9,550
1H-1*	125	9/20/2012	1.125	0.125	82.37	–146	0.00	0.00	35,381	18.85	22.88	7,217
1H-1*	150	9/20/2012	1.15	0.15	107.58	242	0.61	0.57	41,586	22.15	20.59	5,909
1H-1*	175	9/20/2012	1.175	0.175	106.35	101	0.26	0.24	43,714	23.29	21.90	6,345
1H-1*	200	9/20/2012	1.2	0.2	94.20	222	0.56	0.60	40,227	21.43	22.75	6,746
1H-1*	225	9/20/2012	1.225	0.225	99.85	18	0.05	0.05	37,076	19.75	19.78	6,266
1H-1*	250	9/20/2012	1.25	0.25	99.47	118	0.30	0.30	35,159	18.73	18.83	6,167
1H-1*	275	9/20/2012	1.275	0.275	96.11	105	0.27	0.28	34,701	18.49	19.23	6,831
1H-1*	300	9/20/2012	1.3	0.3	95.69	–166	0.00	0.00	34,425	18.34	19.16	6,130
1H-1*	325	9/20/2012	1.325	0.325	92.35	–61	0.00	0.00	31,968	17.03	18.44	6,566
1H-1*	350	9/20/2012	1.35	0.35	100.10	–137	0.00	0.00	31,104	16.57	16.55	6,879
1H-1*	375	9/20/2012	1.375	0.375	103.30	–89	0.00	0.00	33,026	17.59	17.03	6,634
1H-1*	400	9/20/2012	1.4	0.4	101.32	–66	0.00	0.00	31,896	16.99	16.77	5,777
1H-1*	425	9/20/2012	1.425	0.425	104.41	31	0.08	0.08	30,084	16.03	15.35	5,463
1H-1*	450	9/20/2012	1.45	0.45	104.42	–24	0.00	0.00	23,121	12.32	11.80	5,300
1H-1*	475	9/20/2012	1.475	0.475	104.45	–41	0.00	0.00	24,051	12.81	12.27	5,218
1H-1*	500	9/20/2012	1.5	0.5	99.86	–69	0.00	0.00	23,024	12.27	12.28	5,762
1H-1*	525	9/20/2012	1.525	0.525	93.20	140	0.35	0.38	20,591	10.97	11.77	6,168
1H-1*	550	9/20/2012	1.55	0.55	86.75	–98	0.00	0.00	20,189	10.75	12.40	6,963
1H-1*	575	9/20/2012	1.575	0.575	101.25	–117	0.00	0.00	28,243	15.05	14.86	5,823
1H-1*	600	9/20/2012	1.6	0.6	85.96	–2	0.00	0.00	21,225	11.31	13.15	6,784
1H-1*	625	9/20/2012	1.625	0.625	96.94	137	0.35	0.36	27,568	14.69	15.15	6,344
1H-1*	650	9/20/2012	1.65	0.65	96.30	13	0.03	0.03	26,857	14.31	14.86	6,873
1H-1*	675	9/20/2012	1.675	0.675	96.39	–101	0.00	0.00	25,476	13.57	14.08	6,091
1H-1*	700	9/20/2012	1.7	0.7	97.56	–98	0.00	0.00	23,686	12.62	12.93	6,394
1H-1*	725	9/20/2012	1.725	0.725	95.54	–89	0.00	0.00	28,644	15.26	15.97	6,482
1H-1*	750	9/20/2012	1.75	0.75	91.02	175	0.44	0.49	26,896	14.33	15.74	6,646
1H-1*	775	9/20/2012	1.775	0.775	86.75	–87	0.00	0.00	22,932	12.22	14.08	7,080
1H-1*	800	9/20/2012	1.8	0.8	86.81	70	0.18	0.20	25,358	13.51	15.56	7,735
1H-1*	825	9/20/2012	1.825	0.825	79.65	–117	0.00	0.00	26,569	14.15	17.77	7,749
1H-1*	850	9/20/2012	1.85	0.85	73.55	–44	0.00	0.00	25,291	13.47	18.32	7,516
1H-1*	875	9/20/2012	1.875	0.875	69.44	150	0.38	0.55	29,200	15.56	22.40	8,923
1H-1*	900	9/20/2012	1.9	0.9	65.49	39	0.10	0.15	30,413	16.20	24.74	9,562
1H-1*	925	9/20/2012	1.925	0.925	41.92	38	0.10	0.23	25,171	13.41	31.99	11,508
1H-1*	950	9/20/2012	1.95	0.95	49.47	–133	0.00	0.00	22,817	12.15	24.57	9,812
1H-1*	975	9/20/2012	1.975	0.975	41.60	229	0.58	1.39	24,555	13.08	31.44	11,090
1H-1*	1,000	9/20/2012	2	1	30.32	181	0.46	1.51	19,513	10.39	34.28	11,206
1H-1*	1,025	9/20/2012	2.025	1.025	41.34	465	1.17	2.84	31,520	16.79	40.62	11,684
1H-1*	1,050	9/20/2012	2.05	1.05	39.39	326	0.82	2.09	29,932	15.95	40.48	11,831
1H-1*	1,075	9/20/2012	2.075	1.075	45.77	571	1.44	3.15	40,392	21.52	47.01	11,794
1H-1*	1,100	9/20/2012	2.1	1.1	44.46	444	1.12	2.52	39,131	20.85	46.89	11,577
1H-1*	1,125	9/20/2012	2.125	1.125	49.95	724	1.83	3.66	46,179	24.60	49.25	10,942
1H-1*	1,150	9/20/2012	2.15	1.15	54.37	1017	2.57	4.73	46,988	25.03	46.04	11,628
1H-1*	1,175	9/20/2012	2.175	1.175	50.80	541	1.37	2.69	41,583	22.15	43.61	11,323
1H-1*	1,200	9/20/2012	2.2	1.2	52.62	687	1.74	3.30	41,239	21.97	41.75	11,002
1H-1*	1,225	9/20/2012	2.225	1.225	49.92	708	1.79	3.58	37,458	19.95	39.97	11,221
1H-1*	1,250	9/20/2012	2.25	1.25	42.20	452	1.14	2.71	31,993	17.04	40.38	11,216
1H-1*	1,275	9/20/2012	2.275	1.275	47.69	609	1.54	3.23	31,515	16.79	35.20	11,249
1H-1*	1,300	9/20/2012	2.3	1.3	48.88	163	0.41	0.84	33,025	17.59	35.99	10,357
1H-1*	1,325	9/20/2012	2.325	1.325	39.16	456	1.15	2.94	30,855	16.44	41.98	11,512
1H-1*	1,350	9/20/2012	2.35	1.35	45.04	203	0.51	1.14	26,385	14.06	31.20	10,343
1H-1*	1,375	9/20/2012	2.375	1.375	35.13	–16	0.00	0.00	21,459	11.43	32.54	11,246
1H-1*	1,400	9/20/2012	2.4	1.4	35.84	346	0.87	2.44	31,992	17.04	47.56	10,927
1H-1*	1,425	9/20/2012	2.425	1.425	31.88	543	1.37	4.30	28,565	15.22	47.74	11,238
1H-1*	1,450	9/20/2012	2.45	1.45	38.55	550	1.39	3.60	27,729	14.77	38.32	10,873
1H-2*	25	9/20/2012	2.525	1.525	45.68	858	2.17	4.75	47,690	25.40	55.62	10,161

* = data used in the calculation of NMS values and in the splice. All data are included, however, in the event that the splice is modified and NMS values need to be recalculated. Only a portion of this table appears here. The complete table is available in **ASCII** and in Microsoft Excel format (see RAWXRF_U1337.XLS in RAWXRF in **"Supplementary material."**)

Table T4. Shipboard weight percent and calculated area medians for sedimentary components at each site used in calculating final normalized median-squared values, Sites U1335–U1337.

Component	Site U1335		Site U1336		Site U1337	
	Shipboard (wt%)	Calculated area	Shipboard (wt%)	Calculated area	Shipboard (wt%)	Calculated area
Al_2O_3	0.420	232	0.222	125	0.720	285
SiO_2	9.030	32,831.5	4.570	19,713	25.085	47,089.5
K_2O	0.110	3,296	0.046	2,105	0.198	5,350
$CaCO_3$	72.277	2,504,943	87.625	2,497,635	70.136	1,996,713
TiO_2	0.070	2,020	0.019	1,296	0.143	1,691
MnO	0.050	3,366.5	0.089	4,740	0.181	9,542.5
Fe_2O_3	0.470	29,862	0.427	35,612	0.730	43,429
$BaSO_4$	0.301	5,551	0.235	3,139	0.549	7,507

Medians of shipboard data were for all points measured at each site.

Table T5. Age, depth, and stratigraphic data, Sites U1335–U1337.

Datum	Age (Ma)	Site U1335 depth (mcd)	Site U1336 depth (mcd)	Site U1337 depth (mcd)
T *Pseudoemiliania lacunosa*	0.44	2.34		5.84
C1r.2r–C2n	1.778	10.545		27.23
C2An.2n–C2An.2r	3.207	17.735		47.98
C3n.1r–C3n.2n	4.493	23.885		78.31
C3n.4n–C3r	5.235	29.82		94.47
C3An.2n–C3Ar	6.733	40.03		129.805
T *Discoaster hamatus*	9.69	66.115		192.985
T *Coronocyclus nitescens*	12.12	94.95	1.36	258.305
C5ADn–C5ADr	14.581	156.675	30.205	
Tc *Discoaster deflandrei*	15.66	180.6	33.705	357.87
C5Cn.1r–C5Cn.2n	16.256	191.06	46.13	
Bc *Sphenolithus heteromorphus*	17.71	206.33		390.5
B *Sphenolithus belemnos*	19.03	236.92	84.135	412.32

Both biostratigraphic and magnetostratigraphic points were used. T = top, Tc = top common, Bc = bottom common, B = bottom.